Spatial Disposition of Dye Molecules within Metal Oxide Nanotubes

Hirohmi Watanabe and Toyoki Kunitake*

Spatio-Temporal Function Materials Research Group, Frontier Research System (FRS), The Institute of Physical and Chemical Research (RIKEN), Hirosawa 2-1, Wako-shi, Saitama, 351-0198 Japan

Received February 25, 2008. Revised Manuscript Received May 2, 2008

Donor/acceptor systems for electron and energy transfer are fabricated within modified multilayer nanotubes by taking advantage of the precise layering of the surface sol−gel method. Molecular thick layers of dye-embedded metal oxides were successively fabricated on the pore of anodized aluminum oxide (AAO) membrane, and multilayered nanotubes were formed after removal of the AAO template by alkali treatment. The efficiency of interlayer electron/energy transfer was strongly dependent on the distance of the two, and an adequate number of layers of zirconia was sufficient to functionally separate the two active layers. Electron transfer from an immobilized rhodamine B unit to the inner titania layer was prevented by the three zirconia layers as a 2.8 nm thick spacer. On the other hand, five layers of zirconia (4.7 nm) effectively prevented energy transfer from the fluorescamine-embedded outer layer to the rhodamine-B−isothiocyanate-embedded inner layer, in agreement with the quenching radius of the system. These spatially designed nanotubes will be a useful tool for fabricating novel molecular devices.

Introduction

Nano-objects, such as nanotubes, nanoparticles, and nanowires, are major components of the architecture in nanoscience and technology. Particularly, nanotubes are the most popular materials for use because of their unique physical and chemical properties: one-dimensional (1-D) elongated geometry, high surface-to-volume ratio, accessibility to inner and outer surfaces, and unique electronic metal/semiconductor properties. Carbon nanotubes have been targets of intensive research due to their highly interesting mechanical and electronic properties.[1–5] Unfortunately, the structural complexity and difficulty of physical and chemical modification sometimes restrict ready applications of these characteristic properties. Inorganic nanotubes such as tungsten(IV) sulfide, titanium dioxide, and zinc oxide have also been synthesized and extensively studied.[6–9] The template-based fabrication of nanotubes is an additional methodology to prepare functional nanotubes. Precursor materials are coated on the wall of template, and nanotubes are fabricated as replica upon removal of the template. This technique realizes fabrication of a variety of functional nanotubes from polymers,[10–12] metals,[13] semiconductors,[14] inorganic oxides,[6,15,16] and their composites.[17,18]

Incidentally, LbL assembly is known as a candidate technique to grow uniform layers of varying compositions with controlled thickness (nanometer resolution).[19–24] This technique is also useful for synthesizing template-based nanotubes. For example, Ai and co-workers reported the fabrication of an organic nanotube using LbL assembly of poly(allylamine hydrochloride) (PAH) and poly(styrene sulfonic acid) (PSS).[21] We also reported the fabrication of a template-synthesized organic/inorganic composite nanotube by alternate LbL assembly of poly(acrylic acid) and zirconia.[25,26] A representative advantage of the LbL assembled multilayer is to fabricate formation of spatially controlled functions. Since these individual layers are spatially isolated from each other with controlled thickness, different functional units can be continuously and/or dis-

* To whom correspondence should be addressed. E-mail: kunitake@ruby.ocn.ne.jp.

(1) Iijima, S. *Nature* **1991**, *354*, 56–58.
(2) Fukushima, T.; Kosaka, A.; Ishimura, Y.; Yamamoto, T.; Takigawa, T.; Ishii, N.; Aida, T. *Science* **2003**, *300*, 2072–2074.
(3) Zhang, M.; Fang, S.; Zakhidov, A. A.; Lee, S. B.; Aliev, A. E.; Williams, C. D.; Atkinson, K. R.; Baughman, R. H. *Science* **2005**, *309*, 1215–1219.
(4) Guldi, D. M.; Rahman, G. M. A.; Zrtbetto, R.; Prato, M. *Acc. Chem. Res.* **2005**, *38*, 871–878.
(5) Tasis, D.; Tagmatarchis, N.; Bianco, A.; Prato, M. *Chem. Rev.* **2006**, *106*, 1105–1136.
(6) Hoyer, P. *Langmuir* **1996**, *12*, 1411–1413.
(7) Mackie, E. B.; Galvan, D. H.; Aden, E.; Talapatra, S.; Yang, G.; Migone, A. D. *Adv. Mater.* **2000**, *12*, 495–498.
(8) Dloczik, L.; Engelhardt, R.; Ernst, K.; Fiechter, S.; Sieber, I.; Könenkamp, R. *Appl. Phys. Lett.* **2001**, *78*, 3687.
(9) Remškar, M. *Adv. Mater.* **2004**, *16*, 1497–1504.
(10) Yang, X.; Dai, T.; Zhu, Z.; Lu, Y. *Polymer* **2007**, *48*, 4021–4027.
(11) Chen, G.; Soper, S. A.; McCarley, R. *Langmuir* **2007**, *23*, 11777–11781.
(12) Shane, M.; Daniela, I.; O'Carroll, D.; Pierre, L.; Gareth, R. *Chem. Mater.* **2008**, *20*, 996.
(13) Mu, C.; Yu, Y.; Wang, R.; Wu, K.; Xu, D.; Guo, G. *Adv. Mater.* **2004**, *16*, 1550–1553.
(14) Niu, H.; Gao, M. *Angew. Chem., Int. Ed.,* **2006**, *45*, 6462–6466.
(15) You, A.; Lu, G. Q. M.; Gentle, I. R. *Adv. Funct. Mater.* **2007**, *17*, 2600–2605.
(16) Richter, C.; Wu, Z.; Panaitescu, E.; Willey, R. J.; Menon, L. *Adv. Mater.* **2007**, *19*, 946–948.
(17) Shenton, W.; Douglas, T.; Young, M.; Stubbs, G.; Mann, S. *Adv. Mater.* **1999**, *11*, 253.
(18) Mulvihill, M. J.; Rupert, B. L.; He, R.; Hochbaum, A.; Arnold, J.; Yang, P. *J. Am. Chem. Soc.* **2005**, *127*, 16040.
(19) Decher, G. *Science* **1997**, *277*, 1232.
(20) Caruso, F.; Caruso, R. A.; Möhwald, H. *Science* **1998**, *282*, 1111.
(21) Ai, S.; Lu, G.; He, Q.; Li, J. *J. Am. Chem. Soc.* **2003**, *125*, 11140.
(22) Liang, Z.; Susha, A.; Yu, A.; Caruso, F. *Adv. Mater.* **2003**, *15*, 1849.
(23) Tian, Y.; He, Q.; Cui, Y.; Tao, C.; Li, J. *Chem. Eur. J.* **2006**, *12*, 4808.
(24) Tian, Y.; He, Q.; Cui, Y.; Li, J. *Biomacromolecules* **2006**, *7*, 2539.
(25) Huang, J.; Kunitake, T. *Chem. Commun.* **2005**, *21*, 2680.
(26) Huang, J.; Kunitake, T. *J. Mater. Chem.* **2006**, *16*, 4257.

10.1021/cm800549n CCC: $40.75
Published on Web 07/01/2008

Scheme 1. Schematic Diagram of the Fabrication of Nanotubes

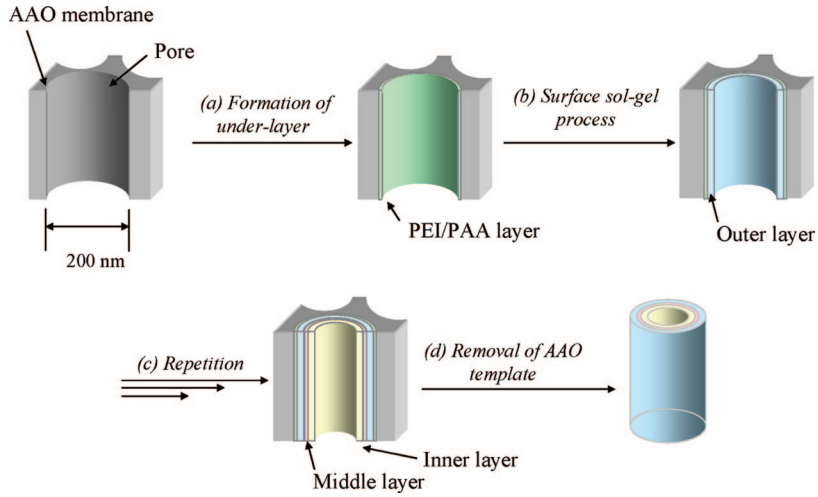

continuously constructed in the multilayered structure. Unfortunately, this fabrication process does not ensure that the intended disposition actually exists in the nanotube. Use of a simple chemical/physical processes is desirable for confirmation of the film design. In this work, we demonstrate that the electron/energy-transfer process within the multilayered nanotube is a useful means to examine such spatial disposition. Multilayered structures of various dye-functionalized metal oxides were constructed within the tubular structure, and photochemical experiments were performed. These results should help in construction of novel functional nanoarchitectures as based on the spatial disposition.

Experimental Section

Chemicals. Titanium(IV) tetra-*n*-butoxide [Ti(O-*n*-Bu)$_4$], zirconium(IV) tetraisopropoxide [Zr(O-*i*-Pr)$_4$, 70 wt % in 1-propanol], and 3-(triethoxysilyl)propylamine [APS] were obtained from Gelest. All fluorescent dyes in this study were obtained from Aldrich. Poly(ethyleneimine) [PEI; $M_w = 1.1 \times 10^4$], poly(acrylic acid) [PAA; $M_w = 1.2 \times 10^4$], and poly(styrene) [PS; $M_w = 1.3 \times 10^3$] were purchased from Polymer Source. All solvents in this study were purchased from Kanto Chemicals and used without further purification.

Measurements. UV−vis absorption and fluorescence spectra were recorded on a Shimadzu UV-3100PC UV−vis scanning spectrophotometer and a Jasco FP-6500 fluorescence spectrophotometer, respectively. Attenuated total reflection Fourier transform infrared (ATR-FT-IR) spectroscopic measurements were performed by a Thermo Nicolet Nexus 670 FT-IR spectroscope. Fluorescence microscopic observation was carried out on an Olympus BX60 fluorescence microscope equipped with a CCD camera. Scanning electron microscopic measurements were performed using Hitachi S5200 field emission scanning electron microscope (FE-SEM).

Surface Sol−Gel Process. Zr(O-*i*-Pr)$_4$ was dissolved in ethanol as a 10 mM solution to use for deposition. A fluorescence dye (1 mM) and APS (1 mM) in ethanol were stirred at room temperature for 24 h, and Zr(O-*i*-Pr)$_4$ was added at 10 mM. Ti(O-*n*-Bu)$_4$ (10 mM) in a 2:1 (vol/vol) mixture of toluene and ethanol was used for deposition of the titania layer.

The surface sol−gel process was conducted as follows (Scheme 1): The pore wall of an AAO membrane (Whatman, anodisk 25, 0.2 μm pore size) was first modified with a (PEI/PAA) layer according to our previous procedure, and the outermost surface was then covered by a PAA layer.[25] The PEI/PAA-modified AAO membrane was placed on a suction filtration funnel, and 20 mL of a given metal alkoxide solution was poured into the funnel. After slow suction filtration of the first 10 mL of the solution, the funnel was allowed to stand for more than 10 min. After filtration of the remaining alkoxide solution, the membrane was rinsed immediately by filtration of 30 mL of ethanol. The AAO membrane was then detached from the suction filtration funnel and kept in air for 10 min. These deposition, rinsing, and hydrolysis process was repeated to fabricate layered structures of metal oxide.

Template Removal. Removal of the AAO template was carried out as described before.[25] First, both surfaces of the modified AAO membrane were coated with PS film by heating the PS powder at 120 °C for 5 min. The AAO membrane was then soaked in 6 M aqueous KOH for 6 h to dissolve the alumina template, giving a nanotube array on the PS support. The individual nanotube was isolated by sonication of a bundle of the PS-supported nanotube in 10 mL of ethanol and subsequent spin coating of the suspension on glass.

Results and Discussion

Fabrication of Metal Oxide Nanotubes. Metal oxide nanotubes were fabricated by the surface sol−gel process within the pore of the (PEI/PAA) layer-modified AAO membrane (Scheme 1). AAO membrane is particularly useful as nanotube template because the size and shape of pore arrays are precisely controlled by anodization conditions. Although UV and QCM measurements have been conveniently used to monitor the LbL growth on flat surfaces, they are not suitable for directly following the current assembly process on the pore wall. Thus, we separately confirmed growth of the layered structure on a quartz plate under similar conditions. UV absorption below 240 nm, which is assigned to amorphous zirconia, increased linearly with the cycle of the surface sol−gel process. QCM frequency change also indicated regular mass increase with the number of adsorption steps. Therefore, we assumed that regular LbL assembly proceeded within the pore of AAO.

Subsequently, the structure of the nanotube was investigated by SEM observation. Figure 1a and 1b shows SEM images of AAO array before and after 20 cycles of the surface sol−gel process of Zr(O-*i*-Pr)$_4$. Apparently the size and morphology of the AAO pore were not affected by

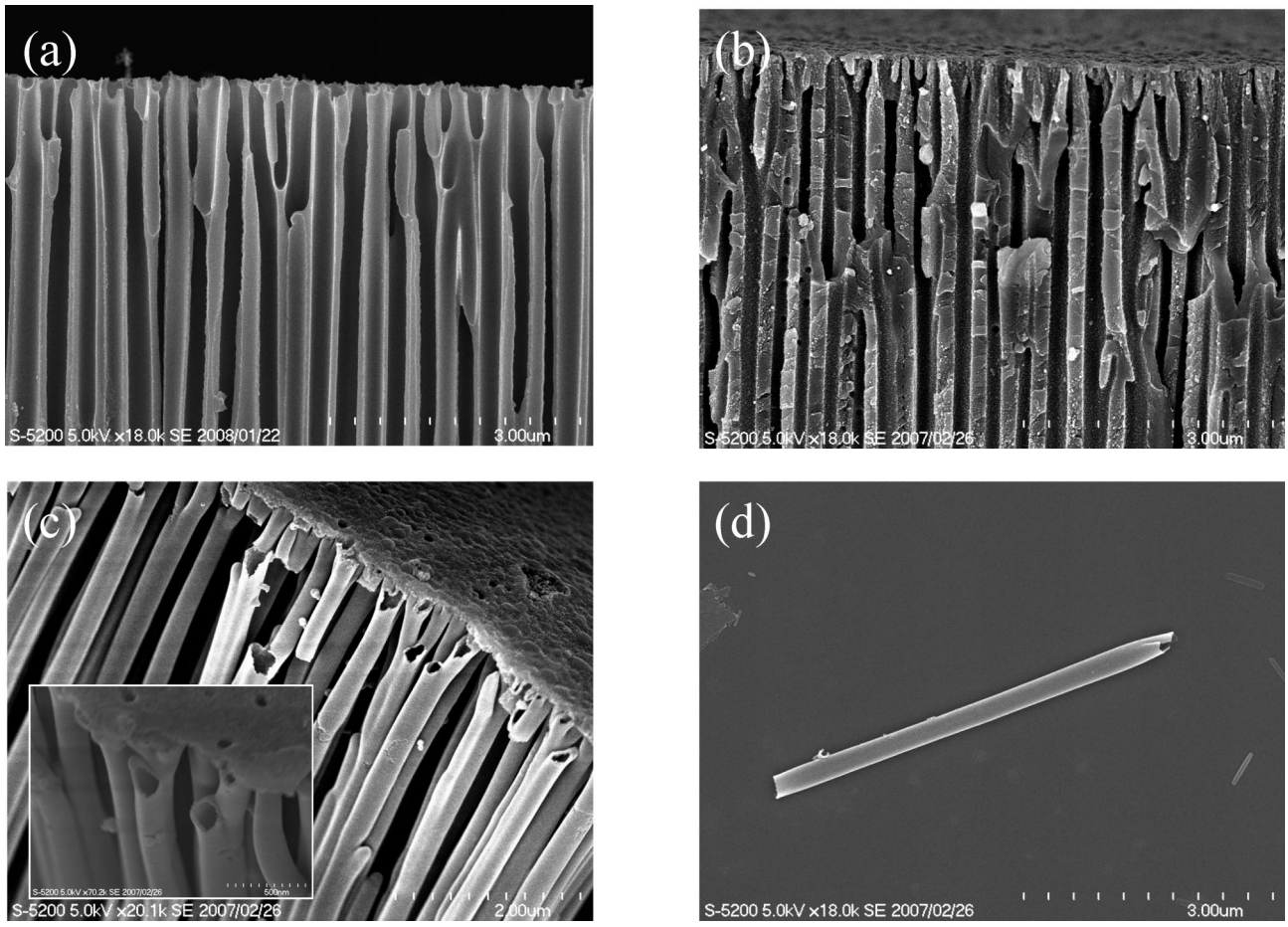

Figure 1. SEM images of the nanotube: (a) cross-section views of AAO template, (b) cross-section views of AAO template after the surface sol−gel process of Zr(O-*i*-Pr)$_4$, (c) nanotube array after removal of AAO template (inset: magnified image), and (d) individual nanotube on glass after removal of the PS support.

the surface sol−gel process. Upon removal of the AAO template by aqueous KOH, formation of zirconia nanotube was clearly seen as in Figure 1c. The tubular structure is formed on PS-support as a replica of the original pore array, and the size of the nanotube (60 μm in length and about 200 nm in the external diameter) was the same as that of the original AAO pore. The external surface of the individual nanotube is very smooth, and its diameter is essentially constant (±5% variation). Replication was performed even in the irregular part of the pore array. The inset of Figure 1c is a magnified image of the edge of the nanotube, and the wall thickness was found to be 25 nm. The thickness of the PEI/PAA underlayer is approximately 1.5 nm as estimated from the literature,[22] and the platinum layer which was sputtered for SEM observation is approximately 5 nm. When these layer thicknesses were subtracted, the individual ZrO_2 layer (20 cycles) of ZrO_2 nanotube is determined to be 0.93 nm. In contrast, the thickness of the individual ZrO_2 layer (20 cycles) on flat quartz plate was determined to be 0.98 nm. It is clear that the surface sol−gel process proceeds within the pore of AAO in the same manner as in the case of flat film. The thickness was also in good agreement with the thickness which was separately determined by the ellipsometric measurements on the flat film (gives a similar value of 1.0 nm).

When the PS-supported nanotube array was sonicated in ethanol for 10 min, the array was detached from the support and dispersed as individual nanotubes. Figure 1d shows the SEM image of a detached nanotube which has been cast on a glass substrate from an ethanol suspension. Although the tubular structure is still maintained, its length is reduced from 60 to 10 μm on average in the course of sonication. The rigid and fragile feature of metal oxide may cause the fragmentation. Use of organic/inorganic composite should be effective for avoiding fragmentation. Alternate LbL assembly of organic polymer layer and metal oxide layer will reinforce the mechanical stability of the nanotube.[25]

Fabrication of Dye-Functionalized Nanotubes. Subsequently, immobilization of functional molecules within the layered nanotube wall was examined. Dye molecules were embedded in the wall by the surface sol−gel process of dye-functionalized (including dye-doped) APS together with Zr(O-*i*-Pr)$_4$. Chemical structures of dye molecules used in this study are shown in Figure 2. When amine-reactive dyes were used for this purpose, formation of a covalent linkage was confirmed by ATR-FT-IR measurement before the surface sol−gel process. Dye-functionalized nanotube was obtained by the surface sol−gel process of two cycles of dye-embedded layer and the additional 20 layers of Zr(O-*i*-Pr)$_4$. Fabrication and isolation process were performed in a way similar to that of the zirconia nanotube in the former section.

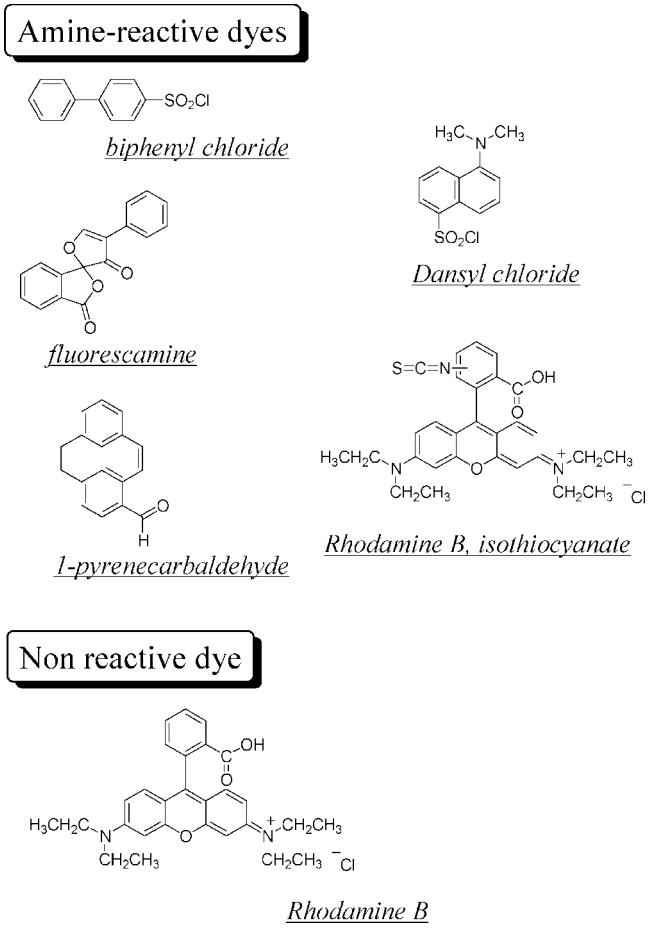

Figure 2. Fluorescent dyes used in this work.

Table 1. Spectroscopic Characteristics of Dye-Functionalized Nanotubes.

amine reactive dye	UV absorption (λ_{max} [nm]) nanotube, flat film[a]	fluorescence emission (λ_{max} [nm]) nanotube, flat film[a,b]
biphenyl chloride	264, 266	349, 346
dansyl chloride	330, 328	505, 499
fluorescamine	*c*, 350	474, 475
rhodamine B, isothiocyanate	550, 553	579, 583

[a] Flat film is the film which is fabricated in a similar procedure on quartz surface. [b] Excitation at 275, 335, 360, and 520 nm for biphenyl chloride, dansyl chloride, fluorescamine, and rhodamine B isothiocyanate, respectively. [c] No specific peaks

Photochemical properties (absorption and fluorescence) of dye-functionalized nanotubes are summarized in Table 1. Spectroscopic measurements of the nanotube were conducted without removing the AAO template in order to avoid scattering of incident light. The λ_{max} values of the emission of dye-functionalized nanotubes were in good agreement with those of the corresponding flat films. We can assume that the molecular environment surrounding the chromophore is essentially unchanged in nanotubes and flat films. On the other hand, the rhodamine-B-doped nanotube did not show any UV and fluorescence peaks of dye molecules. In this case, rhodamine-B molecules are simply dispersed in the metal oxide matrix, and it is not firmly embedded in the matrix. We found that the imine linkage was also not effective for retaining dye molecules in the tube matrix. When 1-pyrenecarboxaldehyde was allowed to react with APS and subjected to the surface sol−gel process, it was not immobilized in the matrix as examined by fluorescence measurement. Apparently, facile hydrolysis of the imine linkage led to loss of the dye during the assembly process. These results clearly indicate that irreversible covalent linkage is necessary for immobilization of dye molecules.

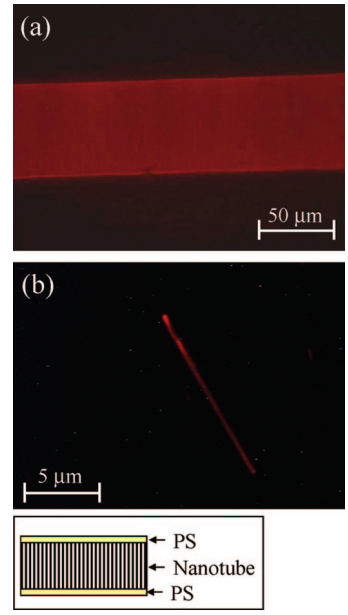

Figure 3. Microscopic image of a rhodamine-B-functionalized nanotube: (a) cross section of the PS-supported nanotube array and (b) individual nanotube on glass after removal of PS support.

The uniform distribution of dye molecules in the nanotube can be confirmed by fluorescence microscopic observation. Figure 3a shows a fluorescence microscopic image of the PS-supported nanotube array that contains rhodamine-B−isothiocyanate-functionalized nanotubes. The sample was excited at around 530−560 nm, and red-colored fluorescence of the rhodamine-B moiety was uniformly seen. Such homogeneous fluorescence images were obtained also from other dye-functionalized nanotube arrays by exciting at the appropriate wavelength. Figure 3b shows a microscopic image of the identical nanotube after dispersion on a glass substrate. Although the nanotube was much shorter than the original one due to fragmentation, the distribution of rhodamine-B molecules was uniform within the nanotube.

Electron Transfer in Designed Multilayer. The current metal oxide nanotube is a convenient scaffold for nanometer-scale separation of functional molecules in the wall which has 1-D elongated geometry. Thus, we constructed an electron-transfer system within the nanotube and investigated its behavior by fluorescence measurements. This nanotube is composed of an outer layer, a middle inert (spacer) layer, and an inner layer, as prepared by the successive surface sol−gel process (see Scheme 1). One layer of rhodamine-B−isothiocyanate-functionalized APS with zirconia was first fabricated as the outer layer. Subsequently, a zirconia layer with a given thickness was fabricated as an inert middle spacer. Then, titania layers were assembled as the inner layer. The frame format of the electron-transferable nanotube together with the corresponding flat film are shown in Figure 4. Titania is a photochemically active material and quenches the fluorescence of the rhodamine-B molecule via an

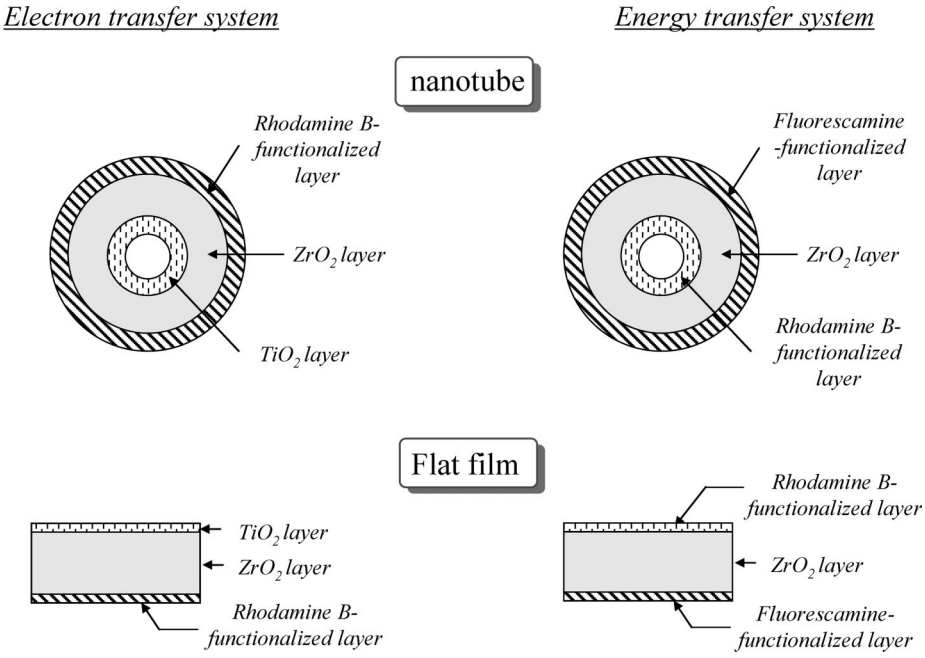

Figure 4. Scheme of the electron/energy-transfer nanotube and the corresponding flat film.

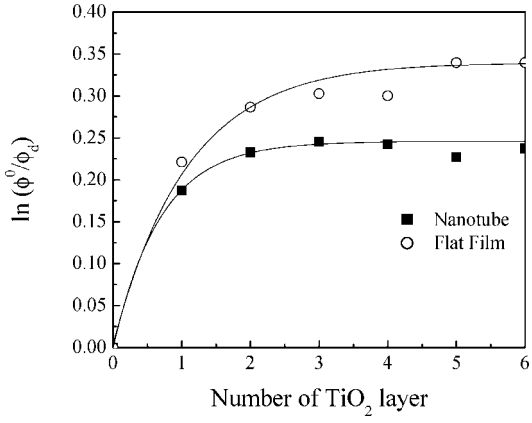

Figure 5. Relationship between the number of inner TiO_2 layers and the ratio of fluorescence intensity (ln $[I^0/I_q]$) of rhodamine-B-functionalized nanotube array (square) and the corresponding flat film (circle).

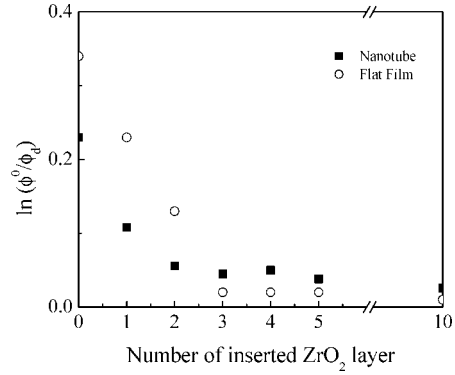

Figure 6. Ratio of fluorescence intensity (ln $[I^0/I_q]$) of rhodamine-B-functionalized nanotube (square) and the corresponding flat film (circle) vs the number of inserted zirconia inert layers.

electron-transfer mechanism.[27] Therefore, rhodamine-B fluorescence at around 540−620 nm could be quenched progressively with increasing number of titania layers and is saturated at three titana layers. Figure 5 shows the relationship between the ratio of fluorescence intensity (ln $[I^0/I_q]$) and the number of titania layers of the nanotube array which has no middle spacer layer. I^0 and I_q are the emission intensity at 550 nm in the absence and presence of titania layers, respectively. The quenching behavior of the corresponding flat film is shown in the same figure. Obviously quenching did not progress completely in both cases, and it was saturated at three titania layers. Actually, a similar saturating behavior is often observed in layered materials such as Langmuir−Blodgett (LB) films and self-assembled multilayers.[28–30] When the donor and acceptor are fixed and spatially separated, electron transfer cannot occur beyond their separation greater than the quenching radius. Thus, saturation is observed even at high concentrations of quencher, in contrast to the case of quenching in solution. The quenching radius can be estimated by changing the average distance between donor and acceptor pairs. Figure 6 shows the relationship between the ratio of fluorescence intensity (ln $[I^0/I_q]$) and the number of inserted zirconia layers. Quenching did not take place any more after insertion of three layers of zirconia. The corresponding flat film also showed an analogous quenching behavior, indicating that the nanotube wall behaves in the same way as that of flat film. As the thickness of each zirconia layer is calculated as 0.93 nm, the quenching radius is roughly estimated as 2.8 nm.

Energy Transfer in Designed Multilayer. Subsequently, an energy-transfer system was constructed within the nanotube. This nanotube consists of three segments: an outer fluorescamine-functionalized layer, a middle zirconia layer,

(27) Bechger, L.; Koenderink, A. F.; Vos, W. L. *Langmuir* **2002**, *18*, 2444.
(28) Murakata, T.; Miyashita, T.; Matsuda, M. *Macromolecules* **1988**, *21*, 2730.
(29) Kondo, T.; Yamada, H.; Nishiyama, K.; Suga, K.; Fujihira, M. *Thin Solid Films* **1989**, *179*, 463.
(30) Kani, R.; Nakano, Y.; Majima, Y.; Hayase, S. *Macromolecules* **1996**, *29*, 4187.

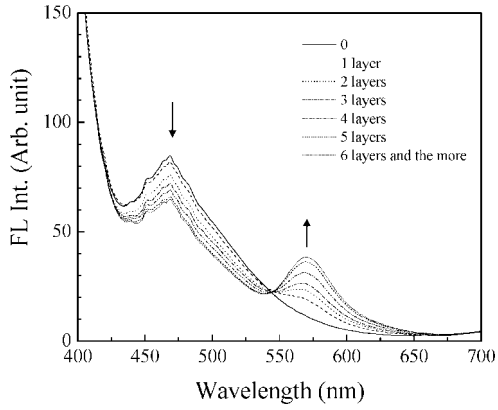

Figure 7. Fluorescence spectra of fluorescamine-functionalized nanotube array according to the assembly of rhodamine-B-functionalized layer (excitation was done at 380 nm, without ziroconia spacer layer).

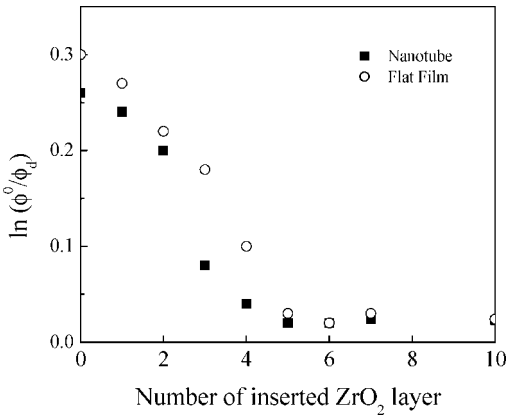

Figure 8. Ratio of fluorescence intensity (ln $[I^0/I_q]$) vs the number of inserted zirconia inert layers: fluorescamine-functionalized nanotube (square) and the corresponding flat film (circle).

and an inner rhodamine-B−isothiocyanate-functionalized layer (Figure 4). The dye-functionalized layer was fabricated by the surface sol−gel process of the corresponding dye-functionalized APS with zirconia. Adequate numbers of zirconia layer were inserted between the outer fluorescamine-embedded layer and the inner rhodamine-B-embedded layer. Figure 7 shows fluorescence spectra of the nanotube array by excitation at 380 nm, where the fluorescamine moiety alone can absorb the light. The nanotube has no middle spacer layer. Upon introduction of the rhodamine-B-functionalized layer, the fluorescence of the fluorescamine moiety at around 440−540 nm was quenched. At the same time, a new peak which originates from the rhodamine-B moiety was observed at around 550−600 nm with an isosbestic point at 545 nm due to energy transfer from the fluorescamine moiety to the rhodamine-B moiety. Because the layered structure is constructed concentrically around the cylindrical axis, photoexcited energy was transported from the external to the internal cylinder of the nanotube. Figure 8 shows the relationship between the ratio of fluorescence intensity (ln $[I^0/I_q]$) and the number of inserted zirconia layers. Quenching due to energy transfer did not take place any more after insertion of five zirconia layers. The quenching behavior was identical between the nanotube system and the corresponding flat film, and the quenching radius of both materials was estimated as 4.7 nm in a way similar to that described in the previous section. It is worth noting that these values of the quenching radius are in good agreement with that of static quenching of fluorescamine and the rhodamine-B−isothiocyanate system in homogeneous PMMA matrix which was separately determined.

Implications and Prospects. Nanomaterial with designed spatial organization is useful for fabrication of high-order functions. In particular, disposition of functional units in nanometer precision is advantageous for such purposes, and multilayering of thin films has been employed frequently. Different functional parts may be placed in separate layers, and their functional cooperativity could produce novel, high-order features. The retinas, for example, possess a layered structure of several nerve cells, and their spatial organization is crucial for conversion of optical information to electric nervous signal.

LbL and LB techniques are effective for artificial fabrication of such multilayered structures, and high-order functional materials for photon-energy conversion, switching, and sensing capabilities were designed based on these techniques. The surface sol−gel process is a promising multilayering technique that is applicable to diverse metal oxides. This technique is based on chemisorption and subsequent hydrolysis of metal alkoxides, and it possesses unique advantages that are not available for other related techniques. In this study, multilayer-modified nanotubes, in which molecularly precise layers are disposed with designed orders, are fabricated. Fluorescence microscopic measurements clearly indicated that the dye-embedded layer was uniformly fabricated on the pore array even after removal of the AAO template. On the other land, dye molecules were not immobilized in metal oxide matrix without covalent linkage. Although the amine-reactive dye used in this study is effective for immobilization, these dyes are limited in kind. We need to develop new types of functional molecules that can be immobilized within the metal oxide layer.

The fundamental processes of electron/energy transfer within the metal oxide nanotube appear to be essentially identical to those in the corresponding flat film. This is because these processes proceed along the thickness direction and the surface curvature does not play a significant role. The unique topological feature of the nanotube may still be effective for other modes of energy/electron transfer. The surface sol−gel process produces disposition of functional units within the metal oxide layer, and the assembled structure creates spatial functionality unlike the conventional system in which functional units are simply distributed without spatial disposition. When these processes proceed across the multilayer organization (along the thickness direction), energy/electron may be collected at the inner part of the tube. A similar energy collection (harvesting) has been observed in core−shell metal nanoparticles.[31–34] Energy is harvested by the three-dimensional shell part to be confined

(31) Creager, S. E.; Collard, D. M.; Fox, M. A. *Langmuir* **1990**, *6*, 1617.
(32) Wargnier, R.; Baranov, A. V.; Maslov, V. G.; Stsiapura, V.; Artemyev, M.; Pluot, M.; Sukhanova, A.; Nabiev, I. *Nano Lett.* **2004**, *4*, 451.
(33) Li, L.; Tedeschi, C.; Kurth, D. G.; Möhwald, H. *Chem. Mater.* **2004**, *16*, 570.
(34) Sudeep, P. K.; Takechi, K.; Kamat, P. V. *J. Phys. Chem. C* **2007**, *111*, 488.

within the central point due to the energy gradient. On the other hand, in the case of nanotubes, the energy/electron flow may be additionally created along the tubular direction. If the nature of the inward process and the longitudinal process is different, it is possible to design novel functional systems by appropriate combination of these processes. Spatially selected functionalization of metal−oxide nanotubes can be achieved through localized dye immobilization. In this respect, metal−oxide nanotubes have unique potentials as scaffolds of nanoprecision devices.

CM800549N